This article has been accepted for publication in IEEE Transactions on Magnetics. This is the author's version which has not been fully edited and content may change prior to final publication. Citation information: DOI 10.1109/TMAG.2026.3704446

Characterizing the Magnetic Gradient Force of Untethered Magnetic Devices Using Two Synchronized Rotating Magnetic Dipoles

Zhengya Zhang[1,2,6], Bohuan Lin[3*], Min Chen[2], Bingxin Huang[4], Anke Klingner[5], Wei Xue[2], Fengping Li[2], Wujun Geng[2*], Sarthak Misra[6,7] and Islam S.M. Khalil[8]

[1]*School of Robot Engineering, Wenzhou University of Technology, Wenzhou, Zhejiang, P.R. China*
[2]*Oujiang Laboratory (Zhejiang Lab for Regenerative Medicine, Vision and Brain Health), Institute of Aging, Key Laboratory of Alzheimers Disease of Zhejiang Province, Zhejiang Provincial Clinical Research Center for Mental Disorders, The Affiliated Wenzhou Kangning Hospital, Wenzhou Medical University, Wenzhou, Zhejiang, P.R. China.*
[3]*Department of Foundational Mathematics, Xi'an Jiaotong Liverpool University, Suzhou, Jiangsu, P.R. China*
[4]*Department of Clinical Laboratory, The Second Affiliated Hospital and Yuying Children's Hospital of Wenzhou Medical University, Wenzhou, Zhejiang, P.R. China*
[5]*Department of Physics, The German University in Cairo, Cairo, Egypt*
[6]*Surgical Robotics Laboratory, Department of Biomaterials & Biomedical Technology, University of Groningen and University Medical Center Groningen, Groningen 9713 AV, The Netherlands*
[7]*Surgical Robotics Laboratory, Department of Biomechanical Engineering, University of Twente, Enschede 7500 AE, The Netherlands*
[8]*Robotics and Mechatronics Research Group, University of Twente, Enschede 7500 AE, The Netherlands*
[*]*Corresponding author: Bohuan Lin (bohuan.lin@xjtlu.edu.cn); Co-corresponding author: Wujun Geng (gengwujun@126.com)*

***Abstract*—Great care is required when employing two-dipole magnetic actuation systems to navigate Untethered Magnetic Devices (UMDs) in *in vivo* medical applications, as uncontrolled gradient forces may lead to tissue trauma or damage. Therefore, it is critical to evaluate the full range of forces that may act on UMDs during operation. This paper introduces a novel method for estimating the upper and lower bounds of the maximal magnetic gradient force acting on UMDs under the influence of two synchronized rotating magnetic dipoles. This study investigates the characteristics of the magnetic gradient force generated by a single rotating dipole and by two synchronized rotating dipoles. The results demonstrate that two synchronized dipoles are more likely to produce an approximately gradient-free region than a single dipole. Within this gradient-free region, the synchronized dipoles were robotically controlled to navigate a UMD inside an agar gel phantom. Closed-loop motion control experiments revealed that the maximum tracking error of a helical UMD actuated by two robotically controlled synchronized rotating dipoles was 3.89 mm.**

***Index Terms*—Magnetic dipoles, Synchronized rotating, Magnetic gradient force, Tetherless magnetic devices**

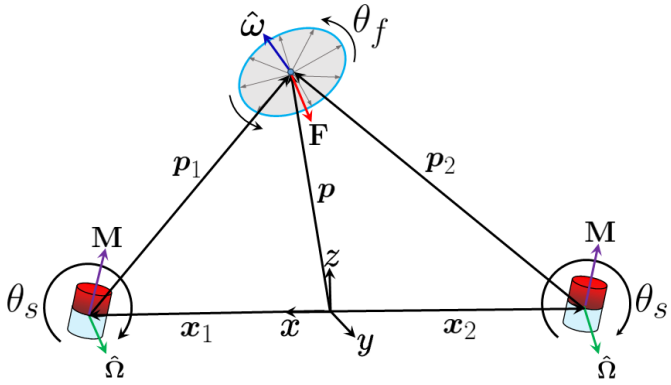

Fig. 1: A superimposed rotating magnetic field is generated using two identical rotating magnetic dipoles. The magnetic dipoles are situated at positions $\boldsymbol{x}_1$ and $\boldsymbol{x}_2$, with each dipole having a magnetic moment $\mathbf{M}$. Each of the magnetic moments has the same magnitude, and they are maintained to be parallel. The magnetic dipoles are controlled to rotate synchronously about a common dipole-rotation axis, $\hat{\mathbf{\Omega}}$ (illustrated by the green arrows), with $\mathbf{M}$ perpendicular to $\hat{\mathbf{\Omega}}$. The rotation angles of the dipoles are denoted by θ_s. The resulting magnetic field at position $\boldsymbol{p}$ undergoes rotation around a distinct field-rotation axis, $\hat{\boldsymbol{\omega}}$ (represented by the red arrow), with its rotation angle defined as θ_f.

I. Introduction

TETHERLESS magnetic devices (UMDs) can be remotely and wirelessly actuated, enabling them to access biological tissues that are challenging to reach using conventional surgical instruments. Leveraging this capability, they hold significant potential to address various medical challenges, including diagnostics [1][2], thrombosis removal [3][4], and targeted drug delivery [5][6]. The primary actuation mechanism for UMDs can involve either the magnetic torque exerted by a rotating magnetic field or the magnetic gradient force produced by a non-uniform magnetic field [7]. The magnetic field generated by rotating magnetic dipoles is inherently non-uniform, inducing a magnetic gradient force on the UMD. This gradient force plays a critical role in influencing the motion control of the UMD, affecting its trajectory and stability during operation. Therefore, it is desirable to harness the benefits of the gradient force on the UMD's motion control while minimizing its adverse effects. To this end, researchers have explored various approaches.

In terms of harnessing the benefits of magnetic gradient forces, Zimmermann *et al.* proposed a methodology that

integrates the magnetic gradient force and magnetic torque to enable the assembly and manipulation of colloidal UMDs [8]. Son *et al*. reported an actuation system utilizing an array of permanent magnets to create a stable magnetic force trap, enabling the continuous penetration and navigation of a UMD within soft tissues [9]. Mahoney *et al*. introduced a method for converting the magnetic gradient force acting on a rotating UMD into a lateral force by rotating the magnetic dipole along a predefined open-loop trajectory [10]. This technique enhances the rolling velocity of the UMD and shows potential for enabling levitation.

In terms of minimizing the adverse effects of magnetic gradient forces, Mahoney *et al* noted that undesirable magnetic forces on a UMD can be minimized by quickly increasing the distance to the actuator magnet or rotating it above the UMDs step-out frequency when localization or control is lost [11]. Further, Mahoney *et al*. also presented a force reduction strategy to mitigate the risk of excessive magnetic gradient force causing biological tissue damage in clinical applications, by establishing an upper bound for the maximum possible force at any orientation of the dipole moment of rotating permanent magnet (RPM) at the UMD's position over one RPM revolution [12]. This strategy establishes an upper bound on the maximum gradient force achievable at any orientation of the RPM dipole moment when subjected to a single rotating dipole. To the best of our knowledge, no prior work has addressed the challenge of quantifying the upper bound of the maximum magnetic gradient force—considering all possible orientations of the RPM dipole moment over a full revolution—in the presence of two synchronized rotating dipoles. Although two synchronized dipoles can eliminate the lateral components of the magnetic gradient force at the center compared to a single rotating dipole [13], the magnetic gradient force cannot be entirely eliminated and must still be evaluated. To bridge this gap, the present study introduces a novel analytical framework for estimating both the upper and lower bounds of the maximum magnetic force acting on UMDs influenced by two synchronized rotating dipoles.

In this paper, we investigate the magnetic gradient force acting on a UMD subjected to two synchronized rotating magnetic dipoles. The letter is organized as follows: Section **II** introduces an iterative method for calculating the maximum magnetic gradient force acting on the UMD under the influence of two synchronized rotating magnetic dipoles. Section **III** presents a novel approach to estimate the upper and lower bounds of the maximum magnetic gradient force produced by the actuation magnets rotating with any given rotation axis, in the presence of two synchronized rotating dipoles acting on a UMD. Section **IV** compares the maximum and average magnetic gradient forces exerted on a UMD in the configurations of a single rotating dipole and two synchronized rotating dipoles. Section **V** describes the closed-loop motion control experiments of UMD in an approximately gradient-free region between two synchronized rotating dipoles, and Section **VI** provides the concluding remarks.

II. Magnetic Gradient Force

Suppose a pair of identical magnets for actuation are synchronized to rotate with identical dipole moment $\mathbf{M}$. Fig. 1 shows the configuration (of the dipoles). Denote by $\mathbf{B}_i$ the magnetic field generated by dipole i, then at position $\boldsymbol{p}$,

$$\mathbf{B}_i = \frac{\mu_0}{4\pi \left\|\boldsymbol{p}_i\right\|^3}(3\hat{\boldsymbol{p}}_i\hat{\boldsymbol{p}}_i^{\mathrm{T}} - \mathbf{I})\mathbf{M}, \quad \text{for} \quad i = 1, 2 \tag{1}$$

where $\mathbf{M}$ is the common dipole moment of the synchronized rotating magnets, $\boldsymbol{p}_i = \boldsymbol{p} - \boldsymbol{x}_i$ with the position $\boldsymbol{x}_i$ of dipole i, $\hat{\boldsymbol{p}}_i = \frac{\boldsymbol{p}_i}{\|\boldsymbol{p}_i\|}$, and μ_0 is the permeability of free space. Further, with $\mathbb{H}_i = 3\hat{\boldsymbol{p}}_i\hat{\boldsymbol{p}}_i^{\mathrm{T}} - \mathbf{I}$, the total magnetic field is

$$\mathbf{B} = \sum_{i=1}^{2}\mathbf{B}_i = \frac{\mu_0 \left\|\mathbf{M}\right\|}{4\pi}\sum_{i=1}^{2}\frac{\mathbb{H}_i}{\left\|\boldsymbol{p}_i\right\|^3}\hat{\mathbf{M}}, \tag{2}$$

where $\hat{\mathbf{M}}$ is the unit vector of $\mathbf{M}$, which changes periodically. Since the magnets rotate synchronously, the magnetic force applied on the UMD is given by $\mathbf{F} = \sum_{i=1}^{2}\nabla(\mathbf{B}_i \cdot \mathbf{m})$, which can be expressed as

$$\mathbf{F} = \frac{3\mu_0 \left\|\mathbf{m}\right\| \left\|\mathbf{M}\right\|}{4\pi}\sum_{i=1}^{2}\frac{1}{\left\|\hat{\boldsymbol{p}}_i\right\|^4}\begin{bmatrix}\hat{\mathbf{M}}^{\mathrm{T}}\mathbb{H}_i^x \\ \hat{\mathbf{M}}^{\mathrm{T}}\mathbb{H}_i^y \\ \hat{\mathbf{M}}^{\mathrm{T}}\mathbb{H}_i^z\end{bmatrix}\hat{\mathbf{m}} = \mathcal{K}\mathbb{F}_{\hat{\mathbf{M}}}\hat{\mathbf{m}}, \tag{3}$$

where matrix $\mathbb{F}_{\hat{\mathbf{M}}}$ is symmetric, as illustrated in APPENDIX A. The vector $\mathbf{m}$ is the dipole moment of the UMD and $\hat{\mathbf{m}}$ is the unit vector of $\mathbf{m}$ and $\mathcal{K} = 3\mu_0 \left\|\mathbf{m}\right\| \left\|\mathbf{M}\right\|/4\pi$, $\mathbb{H}_i^{\mathrm{x}}$ is the matrix mapping $\hat{\mathbf{M}}$ to magnetic field gradient $\nabla\mathbf{B}$ in the $\hat{\mathbf{x}}$ direction. Matrix $\mathbb{H}_i^{\mathrm{x}}$ is given by

$$\mathbb{H}_i^x = (\hat{\mathbf{x}}^{\mathrm{T}}\hat{\boldsymbol{p}}_i)(\mathbf{I} - 5\hat{\boldsymbol{p}}_i\hat{\boldsymbol{p}}_i^{\mathrm{T}}) + \hat{\mathbf{x}}\hat{\boldsymbol{p}}_i^{\mathrm{T}} + \hat{\boldsymbol{p}}_i\hat{\mathbf{x}}^{\mathrm{T}}, \tag{4}$$

and is symmetric. The matrix $\mathbb{H}_i^{\mathrm{y}}$ and $\mathbb{H}_i^z$ are given similarly. In fact, we have the following linear map $\mathbb{G}$:

$$\mathbb{G} : \mathbb{R}^3 \ni \mathbf{M} \mapsto \mathbb{F}_{\mathbf{M}} \in \mathrm{SyM}_3, \tag{5}$$

where SyM_3 denotes the set of all 3×3 symmetric matrices. From (3 and 33) we have:

$$\mathbb{F}_{\hat{\mathbf{M}}} = \sum_{i=1}^{2}\frac{\left(\hat{\boldsymbol{p}}_i\hat{\mathbf{M}}^{\mathrm{T}} + \hat{\mathbf{M}}\hat{\boldsymbol{p}}_i^{\mathrm{T}}\right)}{\left\|\boldsymbol{p}_i\right\|^4} + \sum_{i=1}^{2}\frac{\left(\hat{\mathbf{M}}^{\mathrm{T}}\hat{\boldsymbol{p}}_i\right)\cdot\left(\mathbf{I} - 5\hat{\boldsymbol{p}}_i\hat{\boldsymbol{p}}_i^{\mathrm{T}}\right)}{\left\|\boldsymbol{p}_i\right\|^4} \tag{6}$$

from which the linearity of $\mathbb{G}$ follows directly. Moreover, it is straightforward to check that the trace of $\mathbb{F}_{\hat{\mathbf{M}}}$ is 0.

Suppose that the actuating dipole $\mathbf{M}$ rotates in the plane perpendicular to $\hat{\boldsymbol{\Omega}}$, and dipole $\mathbf{m}$ rotates perpendicularly to $\hat{\omega}$. Here $\hat{\boldsymbol{\Omega}}$ and $\hat{\omega}$ are arbitrary unit vectors in $\mathbb{R}^3$. Let $\hat{\mathbf{M}}_0$ and $\hat{\mathbf{M}}_1$ be an orthonormal basis of the rotation plane of $\hat{\mathbf{M}}$, with $\hat{\mathbf{M}}_1 = \hat{\mathbf{M}}_0 \times \hat{\boldsymbol{\Omega}}$. Note that $\hat{\mathbf{M}}_0$ is user-defined and known. The angle θ_s, defined as the synchronized rotation angle of the magnetic dipole moments, is set to be the angle between $\hat{\mathbf{M}}$ and $\hat{\mathbf{M}}_0$. At the initial moment, $\mathbf{M}$ points vertically upward, corresponding to $\theta_s = 0$. As it rotates clockwise, θ_s increases. Similarly, in the plane of $\mathbf{m}$, we take an orthonormal basis $\hat{\mathbf{m}}_0$ and $\hat{\mathbf{m}}_1$ with $\hat{\mathbf{m}}_1 = \hat{\mathbf{m}}_0 \times \hat{\omega}$. We define that angle θ_f as the rotation angle of the magnetic field at the UMD position. Then the θ_f is set to be the angle between $\hat{\mathbf{m}}$ and $\hat{\mathbf{m}}_0$, and

$\hat{\mathbf{m}}$ can be expressed as

$$\hat{\mathbf{m}} = [\hat{\mathbf{m}}_0 \quad \hat{\mathbf{m}}_1]\mathbf{\Theta_f}, \tag{7}$$

where $\mathbf{\Theta_f} = [\cos\theta_f \quad \sin\theta_f]^{\mathrm{T}}$. Replacing $\hat{\mathbf{m}}$ using (7) in $\hat{\mathbf{m}}^{\mathrm{T}}\mathbb{F}^2_{\hat{\mathbf{M}}}\hat{\mathbf{m}}$ yields

$$\begin{aligned}\hat{\mathbf{m}}^{\mathrm{T}}\mathbb{F}^2_{\hat{\mathbf{M}}}\hat{\mathbf{m}} &= \mathbf{\Theta_f}^{\mathrm{T}}\begin{bmatrix}\hat{\mathbf{m}}_0^{\mathrm{T}}\\ \hat{\mathbf{m}}_1^{\mathrm{T}}\end{bmatrix}\mathbb{F}^2[\hat{\mathbf{m}}_0 \quad \hat{\mathbf{m}}_1]\mathbf{\Theta_f}\\ &= \mathbf{\Theta_f}^{\mathrm{T}}\mathbf{A_f}\mathbf{\Theta_f},\end{aligned} \tag{8}$$

where $\mathbf{A_f}$ is a 2×2 matrix and is given by

$$\mathbf{A_f} = \begin{bmatrix}\hat{\mathbf{m}}_0^{\mathrm{T}}\mathbb{F}^2_{\hat{\mathbf{M}}}\hat{\mathbf{m}}_0 & \hat{\mathbf{m}}_0^{\mathrm{T}}\mathbb{F}^2_{\hat{\mathbf{M}}}\hat{\mathbf{m}}_1\\ \hat{\mathbf{m}}_1^{\mathrm{T}}\mathbb{F}^2_{\hat{\mathbf{M}}}\hat{\mathbf{m}}_0 & \hat{\mathbf{m}}_1^{\mathrm{T}}\mathbb{F}^2_{\hat{\mathbf{M}}}\hat{\mathbf{m}}_1\end{bmatrix}. \tag{9}$$

Let's define λ_f^1 and λ_f^2 as the eigenvalues of matrix $\mathbf{A_f}$, and $\lambda_f^1 \geq \lambda_f^2$. the vector $\mathbf{v_f^1}$ and $\mathbf{v_f^2}$ are the eigenvectors with respect to λ_f^1 and λ_f^2, respectively. The magnetic gradient force is given by

$$\|\mathbf{F}\| = \mathcal{K}\sqrt{\left|\mathbf{\Theta_f}^{\mathrm{T}}\mathbf{A_f}\mathbf{\Theta_f}\right|}. \tag{10}$$

The maximum and minimum magnetic gradient forces for a given direction of $\mathbf{M}$ and any possible orientation of the UMD dipole moment $\mathbf{m}$ at the UMD position $\boldsymbol{p}$ are

$$\|\mathbf{F}(\theta_s)\|_{\max} = \mathcal{K}\sqrt{\lambda_f^1}\ , \tag{11}$$

$$\|\mathbf{F}(\theta_s)\|_{\min} = \mathcal{K}\sqrt{\lambda_f^2}\ . \tag{12}$$

Note that the maximum and minimum magnetic gradient forces applied on a UMD are achieved when $\mathbf{\Theta_f} = \mathbf{v_f^1}$ and $\mathbf{\Theta_f} = \mathbf{v_f^2}$, respectively. Further, the maximum and minimum magnetic gradient forces for any direction of magnetic dipole moment $\mathbf{M}$ and any possible orientation of the UMD dipole moment $\mathbf{m}$ at the UMD position $\boldsymbol{p}$ are given by

$$\|\mathbf{F}\|_{\max} = max\left\{\|\mathbf{F}(\theta_s)\|_{\max}\right\} \tag{13}$$

$$\|\mathbf{F}\|_{\min} = min\left\{\|\mathbf{F}(\theta_s)\|_{\min}\right\} \tag{14}$$

Note that the proposed method to calculate both the maximum and minimum magnetic gradient forces on the UMD is applicable not only to the case of two synchronized rotating magnetic dipoles, but also to the case of a single magnetic dipole. In [12], the maximum magnetic gradient force on UMD for any direction of $\mathbf{M}$ and any orientation of $\mathbf{m}$ at the UMD position $\boldsymbol{p}$ is calculated as $\|\mathbf{F}\|_{\max} = \frac{\kappa}{2}(\|\tilde{\boldsymbol{p}}\| + \sqrt{4 + 5\|\tilde{\boldsymbol{p}}\|^2})$ where $\kappa = 3\mu_0\|\mathbf{m}\|\|\mathbf{M}\|/(4\pi\|\boldsymbol{p}\|^4)$ and $\tilde{\boldsymbol{p}} = (\mathbf{I} - \hat{\mathbf{\Omega}}\hat{\mathbf{\Omega}}^{\mathrm{T}})\hat{\boldsymbol{p}}$. Through comparison, we found that the magnitude of $\|\mathbf{F}\|_{\max}$ calculated using this method is equal to that obtained from Equation (13). This indicates that the two methods for calculating $\|\mathbf{F}\|_{\max}$ are equivalent. Further, the average magnetic gradient force during a single rotation period of magnetic dipoles is defined as

$$\mathbf{F}_{\mathrm{avg}} = \frac{1}{2\pi}\int_0^{2\pi}\mathbf{F}\mathrm{d}\theta_s \tag{15}$$

Thus, the magnetic gradient force acting on the UMD at a specific position can be characterized by its average value as well as the maximum and minimum values of the magnetic gradient force.

III. Estimation of the Bounds of the Maximal Magnetic Gradient Force

We emphasize that a fast estimation of the maximum gradient force is essential when deploying UMDs in *in vivo* medical applications, in order to prevent potential damage to biological tissues. Suppose that $\mathbf{M}$ rotates in Plane $\mathbf{pl_\Omega}$ perpendicular to $\mathbf{\Omega}$, and $\mathbf{m}$ in Plane $\mathbf{pl}_\omega$ perpendicular to ω. Let $\|\mathbf{F}\|_{\max} = \mathcal{K}\|\overline{\mathbf{F}}\|_{\max}$ where $\mathcal{K} = 3\mu_0\|\mathbf{m}\|\|\mathbf{M}\|/4\pi$. Due to the fact that $\mathbb{F}_{\hat{\mathbf{M}}}(\hat{\mathbf{m}}) = \mathbb{F}_{\hat{\mathbf{m}}}(\hat{\mathbf{M}})$, which can be seen directly from (3), the $\|\overline{\mathbf{F}}\|^2_{\max}$ is

$$\begin{aligned}&\max_{\hat{\mathbf{M}},\hat{\mathbf{m}}\in S^2}\left\{\hat{\mathbf{m}}^{\mathrm{T}}\mathbb{F}^2_{\hat{\mathbf{M}}}\hat{\mathbf{m}}\middle|\hat{\mathbf{M}} \perp \hat{\mathbf{\Omega}}, \hat{\mathbf{m}} \perp \hat{\omega}\right\}\\ &\quad= \max_{\hat{\mathbf{M}},\hat{\mathbf{m}}\in S^2}\hat{\mathbf{m}}^{\mathrm{T}}[\hat{\omega}]^{\mathrm{T}}\mathbb{F}^2_{[\hat{\mathbf{\Omega}}]\hat{\mathbf{M}}}[\hat{\omega}]\hat{\mathbf{m}}.\end{aligned} \tag{16}$$

Again, S^2 is compact, and hence the maximum of $\hat{\mathbf{m}}^{\mathrm{T}}\mathbb{F}^2_{\hat{\mathbf{M}}}\hat{\mathbf{m}}$ is attainable, i.e., $\exists\bar{\mathbf{M}}, \bar{\mathbf{m}} \in S^2$ ($\bar{\mathbf{M}}$ and $\bar{\mathbf{m}}$ are unit vectors), s.t.,

$$\|\mathbf{F}\|^2_{\max} = \bar{\mathbf{m}}^{\mathrm{T}}[\hat{\omega}]^{\mathrm{T}}\mathbb{F}^2_{[\hat{\mathbf{\Omega}}]\bar{\mathbf{M}}}[\hat{\omega}]\bar{\mathbf{m}} = \max_{\hat{\mathbf{M}},\hat{\mathbf{m}}\in S^2}\hat{\mathbf{m}}^{\mathrm{T}}[\hat{\omega}]^{\mathrm{T}}\mathbb{F}^2_{[\hat{\mathbf{\Omega}}]\hat{\mathbf{M}}}[\hat{\omega}]\hat{\mathbf{m}}. \tag{17}$$

In particular, it also satisfies $\bar{\mathbf{M}} \perp \hat{\mathbf{\Omega}}$ and $\bar{\mathbf{m}} \perp \hat{\omega}$. Since

$$\bar{\mathbf{m}}^{\mathrm{T}}[\hat{\omega}]^{\mathrm{T}}\mathbb{F}^2_{[\hat{\mathbf{\Omega}}]\bar{\mathbf{M}}}[\hat{\omega}]\bar{\mathbf{m}} = \max_{\mathbf{m}\in S^2}\hat{\mathbf{m}}^{\mathrm{T}}[\hat{\omega}]^{\mathrm{T}}\mathbb{F}^2_{[\hat{\mathbf{\Omega}}]\bar{\mathbf{M}}}[\hat{\omega}]\hat{\mathbf{m}}, \tag{18}$$

it means that $\bar{\mathbf{m}}$ is an eigenvector associated to the largest eigenvalue of the semi-positively definite matrix $[\hat{\omega}]^{\mathrm{T}}\mathbb{F}^2_{[\hat{\mathbf{\Omega}}]\bar{\mathbf{M}}}[\hat{\omega}]$, and then the maximal force with fixed rotation planes $\mathbf{pl_\Omega}, \mathbf{pl}_\omega$ is

$$\|\mathbf{F}\|^2_{\max} = \max_{\hat{\mathbf{M}}\in S^2}\left\{\text{the largest eigenvalue of } [\hat{\omega}]^{\mathrm{T}}\mathbb{F}^2_{[\hat{\mathbf{\Omega}}]\hat{\mathbf{M}}}[\hat{\omega}]\right\}. \tag{19}$$

That is, we need to look for a vector $\bar{\mathbf{M}} \in S^2$ such that $[\hat{\omega}]^{\mathrm{T}}\mathbb{F}^2_{[\hat{\mathbf{\Omega}}]\bar{\mathbf{M}}}[\hat{\omega}]$ has the largest "maximal eigenvalue" among all the other matrices $[\hat{\omega}]^{\mathrm{T}}\mathbb{F}^2_{[\hat{\mathbf{\Omega}}]\hat{\mathbf{M}}}[\hat{\omega}]$.

1) Eigenvalue&Trace of $[\hat{\omega}]^{\mathrm{T}}\mathbb{F}^2_{[\hat{\mathbf{\Omega}}]\hat{\mathbf{M}}}[\hat{\omega}]$*:* Each matrix $[\hat{\omega}]^{\mathrm{T}}\mathbb{F}^2_{[\hat{\mathbf{\Omega}}]\hat{\mathbf{M}}}[\hat{\omega}]$ is semi-positively definite with eigenvector $\hat{\omega}$ associated to eigenvalue 0. Therefore, it has eigenvalues

$$\bar{\nu}_{\hat{\mathbf{M}}} \geq \nu_{\hat{\mathbf{M}}} \geq 0. \tag{20}$$

As a result,

$$\bar{\nu}_{\hat{\mathbf{M}}} \leq \mathrm{trace}[\hat{\omega}]^{\mathrm{T}}\mathbb{F}^2_{[\hat{\mathbf{\Omega}}]\hat{\mathbf{M}}}[\hat{\omega}] \leq 2\cdot\bar{\nu}_{\hat{\mathbf{M}}}. \tag{21}$$

Moreover, there exists an orthonormal eigenbasis $\mathbf{e}_{\bar{\nu}}$, $\mathbf{e}_\nu$ and $\hat{\omega}$ basis with $\mathbf{e}_\nu = [\hat{\omega}]\mathbf{e}_{\bar{\nu}}$, and then

$$\begin{aligned}\mathrm{trace}[\hat{\omega}]^{\mathrm{T}}\mathbb{F}^2_{[\hat{\mathbf{\Omega}}]\hat{\mathbf{M}}}[\hat{\omega}] &= \mathbf{e}_{\bar{\nu}}^{\mathrm{T}}\mathbb{F}^2_{[\hat{\mathbf{\Omega}}]\hat{\mathbf{M}}}\mathbf{e}_{\bar{\nu}} + \mathbf{e}_\nu^{\mathrm{T}}\mathbb{F}^2_{[\hat{\mathbf{\Omega}}]\hat{\mathbf{M}}}\mathbf{e}_\nu\\ &= \mathrm{trace}\mathbb{F}^2_{[\hat{\mathbf{\Omega}}]\hat{\mathbf{M}}} - \hat{\omega}^{\mathrm{T}}\mathbb{F}^2_{[\hat{\mathbf{\Omega}}]\hat{\mathbf{M}}}\hat{\omega}\\ &= \hat{\mathbf{M}}^{\mathrm{T}}[\hat{\mathbf{\Omega}}]^{\mathrm{T}}\mathbb{G}^{\mathrm{T}}\mathbb{G}[\hat{\mathbf{\Omega}}]\hat{\mathbf{M}} - \hat{\mathbf{M}}^{\mathrm{T}}[\hat{\mathbf{\Omega}}]^{\mathrm{T}}\mathbb{F}^2_{\hat{\omega}}[\hat{\mathbf{\Omega}}]\hat{\mathbf{M}}\\ &= \hat{\mathbf{M}}^{\mathrm{T}}[\hat{\mathbf{\Omega}}]^{\mathrm{T}}\left[\mathbb{G}^{\mathrm{T}}\mathbb{G} - \mathbb{F}^2_{\hat{\omega}}\right][\hat{\mathbf{\Omega}}]\hat{\mathbf{M}}.\end{aligned} \tag{22}$$

where the matrix $\mathbb{G}^{\mathrm{T}}\mathbb{G}$ is given in Equation (34). Please refer to APPENDIX B.

Algorithm 1 Procedure for estimating the upper and lower boundaries of maximal gradient force $\|\mathbf{F}\|_{\max}$ exerted on a UMD at position $\boldsymbol{p}$ with given $\hat{\boldsymbol{\Omega}}$ and $\hat{\omega}$ under the actuation of two synchronized rotating magnetic dipoles

1: **Input:** $\hat{\boldsymbol{\Omega}}$, $\hat{\omega}$, and $\boldsymbol{p}$;
2: Construct $[\hat{\boldsymbol{\Omega}}]^{\mathrm{T}}\left[\mathbb{G}^{\mathrm{T}}\mathbb{G}-\mathbb{F}^2_{\hat{\omega}}\right][\hat{\boldsymbol{\Omega}}]$ and get its largest eigenvalue σ with eigenvector $\bar{\mathbf{M}}_\sigma$;
3: Construct $[\hat{\omega}]^{\mathrm{T}}\left[\mathbb{G}^{\mathrm{T}}\mathbb{G}-\mathbb{F}^2_{\hat{\boldsymbol{\Omega}}}\right][\hat{\omega}]$ and get its largest eigenvalue ρ with eigenvector $\mathbf{m}_\rho$;
4: Construct $[\hat{\omega}]^{\mathrm{T}}\mathbb{F}^2_{[\hat{\boldsymbol{\Omega}}]\mathbf{M}_\sigma}[\hat{\omega}]$ and $[\hat{\boldsymbol{\Omega}}]^{\mathrm{T}}\mathbb{F}^2_{[\omega]\mathbf{m}_\rho}[\hat{\boldsymbol{\Omega}}]$;
5: Get the largest eigenvalues $\bar{\nu}_{\mathbf{M}_\sigma}$ of $[\hat{\omega}]^{\mathrm{T}}\mathbb{F}^2_{[\hat{\boldsymbol{\Omega}}]\mathbf{M}_\sigma}[\hat{\omega}]$ and $\bar{\nu}_{\mathbf{m}_\rho}$ of $[\hat{\boldsymbol{\Omega}}]^{\mathrm{T}}\mathbb{F}^2_{[\hat{\omega}]\mathbf{m}_\rho}[\hat{\boldsymbol{\Omega}}]$;
6: Estimate $\|\overline{\mathbf{F}}\|^2_{\max}=\bar{\nu}_{\bar{\mathbf{M}}}=\bar{\nu}_{\bar{\mathbf{m}}}$ with

$$\max\left\{\bar{\nu}_{\mathbf{M}_\sigma},\bar{\nu}_{\mathbf{m}_\rho}\right\}\leq\ \|\overline{\mathbf{F}}\|^2_{\max}\ \leq\min\left\{\sigma,\rho\right\}.$$

7: $\|\mathbf{F}\|_{\max}=\mathcal{K}\|\overline{\mathbf{F}}\|_{\max}$ where $\mathcal{K}=3\mu_0\|\mathbf{m}\|\,\|\mathbf{M}\|/4\pi$;
8: **Output:** The magnitude range of $\|\mathbf{F}\|_{\max}$.

2) Estimation of the largest $\bar{\nu}_{\hat{\mathbf{M}}}$: With $\bar{\nu}_{\hat{\mathbf{M}}}$ denoting the maximal eigenvalue of $[\hat{\omega}]^{\mathrm{T}}\mathbb{F}^2_{[\hat{\boldsymbol{\Omega}}]\hat{\mathbf{M}}}[\hat{\omega}]$, $\bar{\nu}_{\bar{\mathbf{M}}}$ is the largest among all $\bar{\nu}_{\hat{\mathbf{M}}}$, and,

$$\frac{1}{2}\text{trace}[\hat{\omega}]^{\mathrm{T}}\mathbb{F}^2_{[\hat{\boldsymbol{\Omega}}]\bar{\mathbf{M}}}[\hat{\omega}]\leq\ \|\mathbf{F}\|^2_{\max}=\bar{\nu}_{\bar{\mathbf{M}}}\ \leq\text{trace}[\hat{\omega}]^{\mathrm{T}}\mathbb{F}^2_{[\hat{\boldsymbol{\Omega}}]\bar{\mathbf{M}}}[\hat{\omega}]. \tag{23}$$

Let σ be the largest eigenvalue of the matrix $[\hat{\boldsymbol{\Omega}}]^{\mathrm{T}}\left[\mathbb{G}^{\mathrm{T}}\mathbb{G}-\mathbb{F}^2_{\hat{\omega}}\right][\hat{\boldsymbol{\Omega}}]$ and $\hat{\mathbf{M}}_\sigma\in S^2$ an associated eigenvector. Then,

$$\sigma=\hat{\mathbf{M}}^{\mathrm{T}}_\sigma[\hat{\boldsymbol{\Omega}}]^{\mathrm{T}}\left[\mathbb{G}^{\mathrm{T}}\mathbb{G}-\mathbb{F}^2_{\hat{\omega}}\right][\hat{\boldsymbol{\Omega}}]\hat{\mathbf{M}}_\sigma=\text{trace}[\hat{\omega}]^{\mathrm{T}}\mathbb{F}^2_{[\hat{\boldsymbol{\Omega}}]\hat{\mathbf{M}}_\sigma}[\hat{\omega}]$$

and, $\text{trace}[\hat{\omega}]^{\mathrm{T}}\mathbb{F}^2_{[\hat{\boldsymbol{\Omega}}]\bar{\mathbf{M}}}[\hat{\omega}]=\bar{\mathbf{M}}^{\mathrm{T}}[\hat{\boldsymbol{\Omega}}]^{\mathrm{T}}\left[\mathbb{G}^{\mathrm{T}}\mathbb{G}-\mathbb{F}^2_{\hat{\omega}}\right][\hat{\boldsymbol{\Omega}}]\bar{\mathbf{M}}\leq\sigma.$

Let $\bar{\nu}_{\hat{\mathbf{M}}_\sigma}\geq\nu_{\hat{\mathbf{M}}_\sigma}\geq 0$ the eigenvalues of $[\hat{\omega}]^{\mathrm{T}}\mathbb{F}^2_{[\hat{\boldsymbol{\Omega}}]\hat{\mathbf{M}}_\sigma}[\hat{\omega}]$. Since $\bar{\nu}_{\bar{\mathbf{M}}}$ is the largest among all the $\bar{\nu}_{\hat{\mathbf{M}}}$s, it holds

$$\bar{\nu}_{\hat{\mathbf{M}}_\sigma}\leq\bar{\nu}_{\bar{\mathbf{M}}}=\|\mathbf{F}\|^2_{\max}\leq\text{trace}[\hat{\omega}]^{\mathrm{T}}\mathbb{F}^2_{[\hat{\boldsymbol{\Omega}}]\bar{\mathbf{M}}}[\hat{\omega}]\leq\sigma. \tag{24}$$

where $\sigma=\text{trace}[\hat{\omega}]^{\mathrm{T}}\mathbb{F}^2_{[\hat{\boldsymbol{\Omega}}]\hat{\mathbf{M}}_\sigma}[\hat{\omega}]$. That is, $\bar{\nu}_{\hat{\mathbf{M}}_\sigma}$ and σ give a lower bound and an upper bound, respectively, of the maximal force $\|\mathbf{F}\|^2_{\max}=\bar{\nu}_{\bar{\mathbf{M}}}$. Equation (24) provides an estimate of the lower and upper bounds of the maximal gradient force $\|\mathbf{F}\|_{\max}$. Thus, we propose an algorithm to estimate $\|\mathbf{F}\|_{\max}$, which is presented in **Algorithm 1**.

3) Effectiveness validation: To validate the effectiveness of the proposed algorithm, eight spatial points were selected to assess whether the exact maximal gradient forces, computed via the iterative method described in Section II, lie within the interval range predicted by the proposed algorithm. The force magnitudes are evaluated at multiple positions ranging from the origin to points up to $[20\ 20\ 20]^{\mathrm{T}}$ mm. The magnetic gradient forces were calculated theoretically, with the magnetic moments of each dipole and the UMD set to $45.35\ \mathrm{Am}^2$ and $7.5\times10^{-4}\ \mathrm{Am}^2$, respectively.

TABLE I
THE ESTIMATION OF THE UPPER AND LOWER BOUNDS OF MAXIMAL MAGNETIC GRADIENT FORCE APPLIED ON A UMD USING TWO SYNCHRONIZED ROTATING MAGNETIC DIPOLES

$\|\mathbf{F}\|^a_{\max}:\hat{\boldsymbol{\Omega}}\ [0\ 1\ 0]^{\mathrm{T}}$; $\|\mathbf{F}\|^b_{\max}:\hat{\boldsymbol{\Omega}}\ [-\frac{\sqrt{2}}{2}\ \frac{\sqrt{2}}{2}\ 0]^{\mathrm{T}}$

$\boldsymbol{p}$	$[0\ 0\ 0]^{\mathrm{T}}$	$[20\ 0\ 0]^{\mathrm{T}}$	$[0\ 20\ 0]^{\mathrm{T}}$	$[0\ 0\ 20]^{\mathrm{T}}$
$\|\mathbf{F}\|^a_{\max}$	0	21.14	9.43	9.74
UB	0	23.64	9.43	13.34
LB	0	21.14	9.43	9.43
$\|\mathbf{F}\|^b_{\max}$	0	15.79	15.79	9.74
UB	0	17.30	17.30	13.34
LB	0	15.79	15.79	9.43
$\boldsymbol{p}$	$[20\ 20\ 0]^{\mathrm{T}}$	$[20\ 0\ 20]^{\mathrm{T}}$	$[0\ 20\ 20]^{\mathrm{T}}$	$[20\ 20\ 20]^{\mathrm{T}}$
$\|\mathbf{F}\|^a_{\max}$	22.51	23.48	12.71	24.15
UB	24.65	26.86	15.36	27.16
LB	22.51	23.48	12.71	24.15
$\|\mathbf{F}\|^b_{\max}$	31.94	18.65	18.65	32.99
UB	35.71	21.41	21.41	37.33
LB	31.94	18.64	18.64	32.99

UB: Upper Boundary, LB: Lower Boundary; $\|\mathbf{F}\|_{\max}$: μN, $\boldsymbol{p}$: mm

Table I summarizes the estimated upper and lower bounds of maximal gradient force $\|\mathbf{F}\|_{\max}$ acting on a UMD at various positions, under the influence of two synchronized rotating dipoles. The values $\|\mathbf{F}\|^a_{\max}$ and $\|\mathbf{F}\|^b_{\max}$ correspond to the unit vectors of dipole-rotation axis $\hat{\boldsymbol{\Omega}}=[0\ 1\ 0]^{\mathrm{T}}$ and $\hat{\boldsymbol{\Omega}}=[-\frac{\sqrt{2}}{2}\ \frac{\sqrt{2}}{2}\ 0]^{\mathrm{T}}$, respectively. The results demonstrate that the proposed estimation method yields tight bounds across all tested positions, thereby validating the effectiveness and reliability of the proposed approach in predicting the range of maximal magnetic gradient forces under the influence of two synchronized rotating dipoles.

IV. COMPARISON OF MAGNETIC GRADIENT FORCE APPLIED ON UNTETHERED MAGNETIC DEVICES

The magnetic gradient force plays a critical role in influencing the lateral motion of the UMD. To investigate this, we compare the magnetic gradient forces acting on the UMD under the actuation of a single rotating dipole versus two synchronized rotating dipoles.

A. Maximum magnetic gradient force

In Fig. 2, it illustrates the variation of the magnetic gradient force, $\|\mathbf{F}(\theta_s)\|_{\max}$, with respect to the rotation angle of the magnetic dipole moments, θ_s, at different positions $\boldsymbol{p}$. The plots compare the forces exerted on the UMD under two actuation configurations: Single rotating magnetic dipole represented by the blue curves and two synchronized rotating magnetic dipoles represented by the red curves. We observe that the red curves consistently exhibit lower values of $\|\mathbf{F}(\theta_s)\|_{\max}$ compared to the blue curves, indicating lower magnetic gradient forces under the actuation of two synchronized rotating magnetic dipoles.

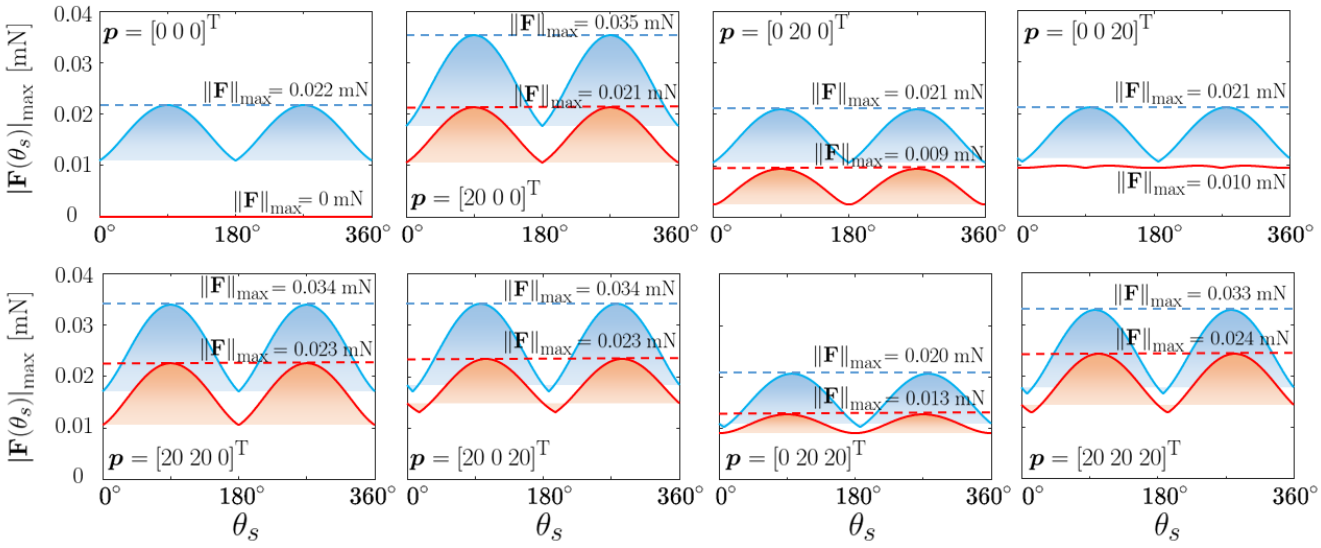

Fig. 2: The variation of $\|\mathbf{F}(\theta_s)\|_{\max}$ with respect to the rotation of magnetic dipole moments at various positions is presented for two actuation configurations. The blue curves correspond to the actuation configuration with a single rotating magnetic dipole located at position $\boldsymbol{x}_1 = [175\ 0\ 0]$ mm, while the red curves represent the actuation configuration with two synchronized rotating magnetic dipoles located at positions $\boldsymbol{x}_1 = [175\ 0\ 0]$ mm and $\boldsymbol{x}_2 = [-175\ 0\ 0]$ mm.

TABLE II
AVERAGE MAGNETIC GRADIENT FORCE

(Units of $\|\mathbf{F}\|_{\mathrm{avg}}$: μN, $\boldsymbol{p}$: mm)

$\boldsymbol{p}$	$[0\ 0\ 0]^{\mathrm{T}}$	$[20\ 0\ 0]^{\mathrm{T}}$	$[0\ 20\ 0]^{\mathrm{T}}$	$[0\ 0\ 20]^{\mathrm{T}}$
$\|\mathbf{F}\|^1_{\mathrm{avg}}$	16.90	27.47	16.42	16.47
$\|\mathbf{F}\|^2_{\mathrm{avg}}$	0	16.50	6.33	8.51
$\boldsymbol{p}$	$[20\ 20\ 0]^{\mathrm{T}}$	$[20\ 0\ 20]^{\mathrm{T}}$	$[0\ 20\ 20]^{\mathrm{T}}$	$[20\ 20\ 20]^{\mathrm{T}}$
$\|\mathbf{F}\|^1_{\mathrm{avg}}$	26.46	26.58	16.00	25.62
$\|\mathbf{F}\|^2_{\mathrm{avg}}$	17.17	18.23	10.21	18.58

B. Average magnetic gradient force

At low actuation frequencies, the magnetic dipoles rotate slowly such that UMD remains synchronized with the rotating magnetic field. In this case, the $\mathbf{m}$ is assumed to approximately align with $\mathbf{B}$ such that

$$\hat{\mathbf{m}} = \hat{\mathbf{B}}. \tag{25}$$

By substituting (3) and (25) into (15), we obtain the average magnetic gradient force acting on the UMD at low actuation frequencies.

In Table II, it summarizes the average magnetic gradient force ($\mathbf{F}_{\mathrm{avg}}$) exerted on the UMD at various positions under the actuation of a single rotating magnetic dipole ($\mathbf{F}^1_{\mathrm{avg}}$) and two synchronized rotating magnetic dipoles ($\mathbf{F}^2_{\mathrm{avg}}$). The positions considered include axial, planar, and three-dimensional locations. We observe that $\mathbf{F}^2_{\mathrm{avg}}$ is generally lower compared to $\mathbf{F}^1_{\mathrm{avg}}$ at corresponding positions, indicating a reduction in the magnetic gradient force under the actuation of the two synchronized rotating magnetic dipoles.

C. Magnetic gradient force in spherical space

The motion of a UMD is influenced by both the rotational axis direction of the magnetic field (ω) and the magnetic gradient force. If the magnetic gradient force in a given space is negligible and does not affect the UMD's trajectory in fluids, the space is termed "gradient-free." In such a gradient-free region, motion control of the UMD is greatly simplified, as there is no need to account for gradient forces. To assess the gradient-free nature of a space, investigating the spatial distribution of magnetic gradient forces acting on UMDs is crucial. For this purpose, a spherical surface with a diameter of 20 mm within the workspace is selected to analyze the distribution of magnetic gradient forces on the UMD. In the actuation configuration with two synchronized rotating dipoles, the spherical surface is centered at the midpoint of the line segment connecting the two magnetic dipoles.

Fig. 3 illustrates the spatial distributions of magnetic gradient forces on the spherical surface, under the actuation of single rotating dipole located at position $\boldsymbol{x}_1 = [175\ 0\ 0]$ mm (Fig. 3(a)) and two synchronized rotating dipoles located at positions $\boldsymbol{x}_1 = [175\ 0\ 0]$ mm and $\boldsymbol{x}_2 = [-175\ 0\ 0]$ mm, respectively. (Fig. 3(d)). The subfigures detail the distribution characteristics of both the maximum and average magnetic gradient forces $\|\mathbf{F}\|_{\max}$ and $\|\mathbf{F}\|_{\mathrm{avg}}$, providing comparative insights between the two actuation configurations. Figs. 3(b) and 3(c) show the distributions of $\|\mathbf{F}\|_{\max}$ and $\|\mathbf{F}\|_{\mathrm{avg}}$ on the spherical surface under the actuation of a single rotating dipole, while Figs. 3(e) and 3(f) illustrate these distributions under the actuation of two synchronized rotating rotating dipoles. Both the maximum and average magnetic gradient forces are observed to be lower and more evenly distributed when two synchronized rotating magnetic dipoles are used. The maximum magnetic gradient force on the spherical surface is 0.035 mN with a single rotating dipole, and 0.021 mN with two synchronized rotating dipoles. These observations lead to the conclusion that the use of two synchronized rotating dipoles results in forming an approximately gradient-free region, as compared to the actuation with a single rotating dipole.

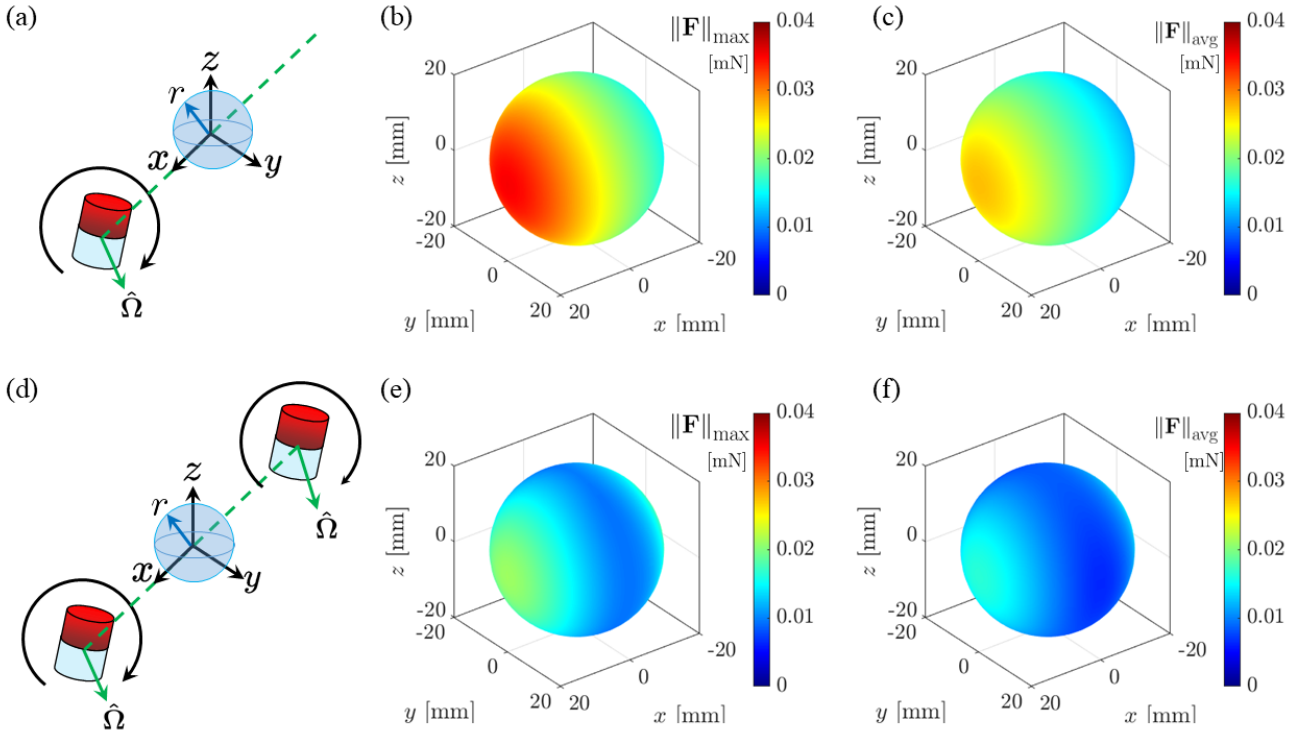

Fig. 3: The magnetic gradient force distributions on a spherical surface for two actuation configurations. (a) Single Rotating Magnetic Dipole located at position $\boldsymbol{x}_1 = [175\ 0\ 0]$ mm: (b) and (c) illustrate the spatial distribution of the maximum and average magnetic gradient forces over the spherical surface under the influence of a single rotating magnetic dipole, respectively. (d) Two Synchronized Rotating Magnetic Dipoles located at positions $\boldsymbol{x}_1 = [175\ 0\ 0]$ mm and $\boldsymbol{x}_2 = [-175\ 0\ 0]$ mm: (e) and (f) display the spatial distribution of the maximum and average magnetic gradient forces under the influence of two synchronized rotating magnetic dipoles, respectively.

V. Closed-Loop Motion Control Experiment

As shown in Fig. 5, the swimming performance of a helical UMD in an agar gel phantom is demonstrated under the actuation of a single rotating magnetic dipole and two synchronized rotating magnetic dipoles. The helical UMD is composed of a helical body and a magnet. The magnet, with a diameter of 1 mm and a height of 1 mm, and a weight of 0.0064 gram, is attached to the end of the helical body. The helical body itself has a length of 4 mm and a diameter of 1.5 mm, and a weight of 0.0049 gram. The helical UMD is controlled to swim in a cubic container (100×100×100 mm) filled with the agar gel phantom for simulating a viscoelastic environment, along with imaging equipment (Aviator GIGE, avA1000-100gm, Basler AG, Ahrensburg, Germany) to monitor the helical UMD's motion.

As a helical UMD approaches either of the magnetic dipoles, it may experience excessive gradient force. This excessive force may potentially result in a loss of motion control of the helical UMD. During the motion control, we make an effort to position the helical UMD within the central region between the two magnetic dipoles. This minimizes the influence of gradient forces on the helical UMD's motion. As illustrated in IV-C, it shows the existence of an approximately gradient-free region when two synchronized rotating dipoles are used, as opposed to a single rotating dipole. In an agar gel phantom, we conducted closed-loop motion control of a 4-mm-long helical UMD using a magnetic dipole-based robotic system without considering the influence of magnetic gradient force on the UMD. This system integrates two synchronized rotating magnetic dipoles with a robotic manipulator, as illustrated in Fig. 4. Each magnetic dipole is driven by a Maxon motor (Planetary Gearhead GP 32 C D32 mm, 1.0-6.0 Nm, Ceramic Version) and controlled by a Maxon EPOS2 drive unit (EPOS2 50/5, digital positioning controller, 5 A, 1150 VDC).

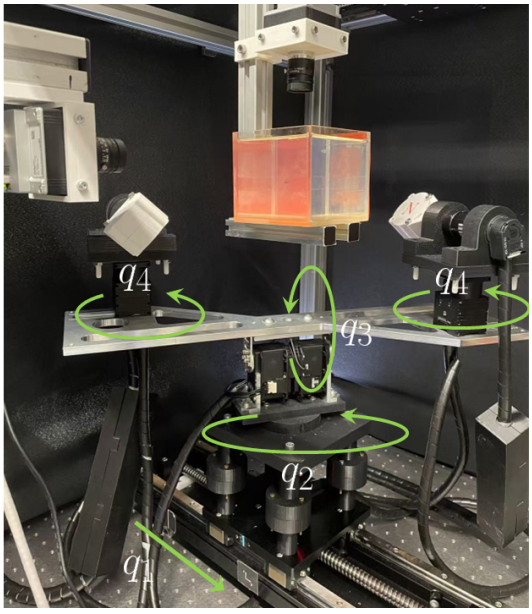

Fig. 4: The magnetic dipole-based robotic system for the closed-loop motion control of UMDs

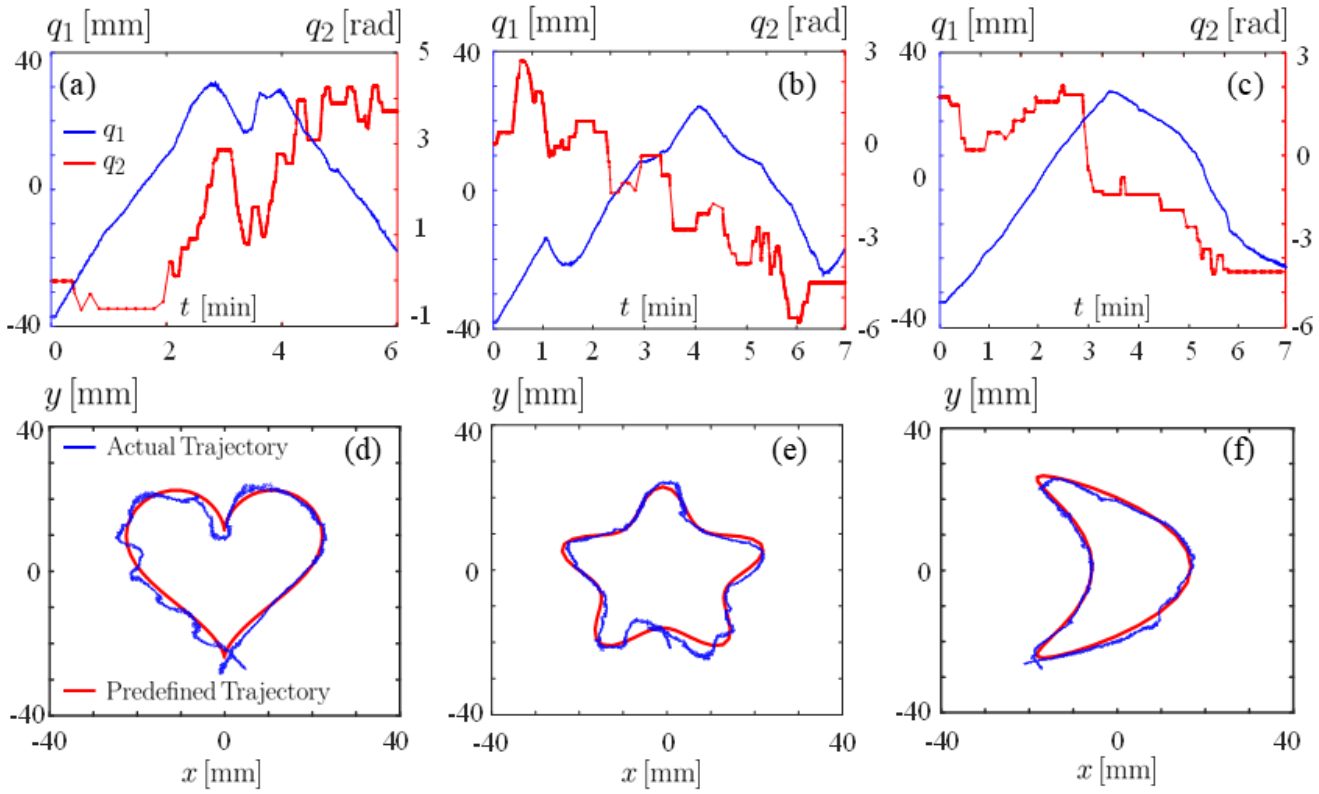

Fig. 5: Closed-loop motion control of a 4-mm-long helical UMD is demonstrated using a magnetic dipole-based robotic system which integrates two synchronized rotating dipoles with a robotic manipulator. In these closed-loop experiments, the control inputs (a), (b), and (c) generate three distinct trajectory patterns: (d) heart-shaped, (e) star-shaped, and (f) crescent-shaped, respectively. In each case, the red trajectory represents the predefined path, while the blue trajectory shows the actual path of the UMD.

The system has four degrees of freedom (DOFs): one translational DOF associated with q_1 and three rotational DOFs associated with q_2, q_3, q_4. The translational motion is realized by a linear stage (KUA1505-520-150-A1-N3, X-axis unit, Japan) driven by an A1 actuator (MX-106R, Dynamixel). The yaw motion corresponding to q_2 is actuated by an A2 actuator (H42P-020-S300-R, Dynamixel PRO PLUS). The pitching motion (q_3) is generated by two A1 actuators operating in synchronous mode, while the second yaw motion (q_4) is driven by two A3 actuators (M42P-010-S260-R, Dynamixel PRO PLUS). The joint-space vector $\mathbf{q}$ is defined as $\mathbf{q} = [q_1, q_2, q_3, q_4]$. The experiments with control inputs involving only q_1 and q_2 (with $q_3 = q_4 = 0$).

A. Determination of the approximately gradient-free region

The size of the approximately gradient-free region can be determined experimentally. The UMD experiences a relatively small magnetic field gradient when it operates in the central region between the two synchronized rotating dipoles. As it moves closer to either dipole, the magnetic field gradient increases, resulting in a larger gradient force and consequently greater deviation from the predefined trajectory. Accordingly, the trajectory tracking error is used as an indicator to characterize the extent of the approximately gradient-free region. To quantify the extent of this region, circular trajectory tracking experiments can be conducted under rotating magnetic fields with different frequencies. At low frequencies, the measured trajectory closely follows the predefined circular path, whereas noticeable deviations are observed at higher frequencies. By gradually increasing the rotating magnetic field frequency, a trajectory can be identified that represents the largest circular area within which the UMD can still track the predefined path with acceptable accuracy. The corresponding circular region is then defined as the approximately gradient-free region.

B. Closed-loop position-error feedback control

A closed-loop position-error feedback controller based on the normalized error direction was proposed for UMD navigation. The trajectory-tracking experiments were conducted by decomposing the predefined trajectory into a sequence of representative waypoints ($\boldsymbol{p}_{ref}$), which were sequentially tracked under the proposed control strategy. At each control step, the position error was calculated as $\mathbf{e} = \boldsymbol{p}_{ref} - \boldsymbol{p}_{act}$ where $\boldsymbol{p}_{act}$ denotes the actual UMD position measured using a camera-based vision system. The normalized error vector $\hat{\mathbf{e}} = \mathbf{e}/\|\mathbf{e}\|$ was then used as the desired motion direction of the UMD. Based on this desired direction, the corresponding desired joint-space vector $\mathbf{q}^d$ was obtained and the robotic system was driven from the current state $\mathbf{q}$ to $\mathbf{q}^d$. This process was repeated until the position error norm $\|\mathbf{e}\|$ was smaller than the prescribed threshold δ_p.

The control inputs shown in Figs. 5(a), 5(b), and 5(c),

effectively realize three distinct predefined trajectory patterns: a heart-shaped trajectory, a star-shaped trajectory, and a crescent-shaped trajectory, as illustrated in Figs. 5(d), 5(e), and 5(f), respectively. For each trajectory pattern, the red and blue lines represent the predefined and actual UMD trajectories, respectively. The maximum tracking error for the three experimental trajectories is 3.89 mm. This demonstrates the system's accuracy and ability to achieve the desired motion patterns through closed-loop control.

VI. Conclusion

In this paper, we propose a novel approach to estimate the upper and lower bounds of the magnetic gradient force for arbitrary orientations of the UMD dipole moment under the influence of two synchronized rotating dipoles. This approach offers a computationally efficient solution to ensure safe magnetic actuation in biomedical applications. A comparative analysis is performed to quantify the magnetic gradient forces at different spatial locations for a single rotating magnetic dipole and for two synchronized rotating magnetic dipoles. We conclude that two synchronized rotating magnetic dipoles are more likely to generate an approximately gradient-free region compared to a single rotating dipole, which benefits the motion control of helical UMDs by removing the influence of magnetic gradient forces. The two synchronized rotating dipoles can be integrated into the end-effector of a manipulator and robotically controlled to navigate the UMD within the approximately gradient-free region.

Although this approach provides an effective means of estimating the force acting on the UMD, its accuracy is influenced by several factors. First, the actuator magnets are modeled using the magnetic dipole approximation, which may introduce deviations when the distance between the magnets and the UMD is not sufficiently large compared with the magnet dimensions. Second, uncertainties in the identified dipole moments and possible position deviations of the actuator magnets can propagate into the calculated gradient force. To evaluate this effect, we analyzed the influence of actuator-magnet position deviations on the magnetic gradient force and derived an upper-bound estimate of the resulting force error. The detailed derivation and error-bound formulation are provided in Appendix C. This analysis helps clarify the expected accuracy and limitations of the proposed force calculation method.

As part of future work, we will investigate the magnetic gradient force acting on UMDs under the influence of three or more synchronized rotating magnetic dipoles. This exploration aims to deepen the understanding of how increasing the number of synchronized dipoles affects the magnitude, direction, and distribution of the magnetic gradient force. By leveraging these insights, we can further optimize the magnetic actuation configurations to enable more precise, predictable, and safe control of UMDs, ultimately advancing their utility in biomedical applications.

Appendix A
Proof of the Symmetry of Matrix $\mathbb{F}_{\hat{\mathbf{M}}}$

Now we derive (6), from which the symmetry of $\mathbb{F}_{\hat{\mathbf{M}}}$ is obvious. First,

$$\begin{bmatrix} \hat{\mathbf{M}}^{\mathrm{T}}\mathbb{H}_i^x \\ \hat{\mathbf{M}}^{\mathrm{T}}\mathbb{H}_i^y \\ \hat{\mathbf{M}}^{\mathrm{T}}\mathbb{H}_i^z \end{bmatrix} = \bar{\mathbf{x}}\hat{\mathbf{M}}^{\mathrm{T}}\cdot\mathbb{H}_i^x + \bar{\mathbf{y}}\hat{\mathbf{M}}^{\mathrm{T}}\cdot\mathbb{H}_i^y + \bar{\mathbf{z}}\hat{\mathbf{M}}^{\mathrm{T}}\cdot\mathbb{H}_i^z. \quad (26)$$

Rewrite $\bar{\mathbf{x}}\hat{\mathbf{M}}^{\mathrm{T}}\cdot\mathbb{H}_i^x$, we obtain

$$\begin{aligned}\bar{\mathbf{x}}\hat{\mathbf{M}}^{\mathrm{T}}\cdot\mathbb{H}_i^x &= \bar{\mathbf{x}}\hat{\mathbf{M}}^{\mathrm{T}}\cdot\left[(\bar{\mathbf{x}}\cdot\hat{\boldsymbol{p}}_i)\big(\mathbf{I}-5\hat{\boldsymbol{p}}_i\hat{\boldsymbol{p}}_i^{\mathrm{T}}\big)+\bar{\mathbf{x}}\hat{\boldsymbol{p}}_i^{\mathrm{T}}+\hat{\boldsymbol{p}}_i\bar{\mathbf{x}}^{\mathrm{T}}\right]\\ &= \bar{\mathbf{x}}\hat{\mathbf{M}}^{\mathrm{T}}\cdot\left[(\bar{\mathbf{x}}\cdot\hat{\boldsymbol{p}}_i)\big(\mathbf{I}-5\hat{\boldsymbol{p}}_i\hat{\boldsymbol{p}}_i^{\mathrm{T}}\big)+\bar{\mathbf{x}}\hat{\boldsymbol{p}}_i^{\mathrm{T}}\right]+\bar{\mathbf{x}}\hat{\mathbf{M}}^{\mathrm{T}}\cdot\hat{\boldsymbol{p}}_i\bar{\mathbf{x}}^{\mathrm{T}}.\end{aligned} \quad (27)$$

For the last term on the right side above,

$$\bar{\mathbf{x}}\hat{\mathbf{M}}^{\mathrm{T}}\cdot\hat{\boldsymbol{p}}_i\bar{\mathbf{x}}^{\mathrm{T}} = \big(\hat{\mathbf{M}}^{\mathrm{T}}\hat{\boldsymbol{p}}_i\big)\cdot\bar{\mathbf{x}}\bar{\mathbf{x}}^{\mathrm{T}} \quad (28)$$

and note that it is a symmetric matrix. For re-expressing the remaining terms, we will resort to the following formula

$$r\cdot\mathbf{v}\mathbf{w}^{\mathrm{T}} = \mathbf{v}\cdot[r]\cdot\mathbf{w}^{\mathrm{T}}, \quad (29)$$

where $\mathbf{v}$ and $\mathbf{w}$ are both $n\times 1$ matrices and $[r]$ is the 1×1 matrix with the only element $r\in\mathbb{R}$.

$$\begin{aligned}&\bar{\mathbf{x}}\hat{\mathbf{M}}^{\mathrm{T}}\cdot\left[(\bar{\mathbf{x}}^{\mathrm{T}}\hat{\boldsymbol{p}}_i)\big(\mathbf{I}-5\hat{\boldsymbol{p}}_i\hat{\boldsymbol{p}}_i^{\mathrm{T}}\big)+\bar{\mathbf{x}}\hat{\boldsymbol{p}}_i^{\mathrm{T}}\right]\\ &= (\bar{\mathbf{x}}^{\mathrm{T}}\hat{\boldsymbol{p}}_i)\bar{\mathbf{x}}\hat{\mathbf{M}}^{\mathrm{T}}\cdot\big(\mathbf{I}-5\hat{\boldsymbol{p}}_i\hat{\boldsymbol{p}}_i^{\mathrm{T}}\big)+\bar{\mathbf{x}}\hat{\mathbf{M}}^{\mathrm{T}}\cdot\bar{\mathbf{x}}\hat{\boldsymbol{p}}_i^{\mathrm{T}}\end{aligned} \quad (30)$$

For the second term:

$$\bar{\mathbf{x}}\hat{\mathbf{M}}^{\mathrm{T}}\cdot\bar{\mathbf{x}}\hat{\boldsymbol{p}}_i^{\mathrm{T}} = \bar{\mathbf{x}}\big(\hat{\mathbf{M}}^{\mathrm{T}}\bar{\mathbf{x}}\big)\hat{\boldsymbol{p}}_i^{\mathrm{T}} = \bar{\mathbf{x}}\big(\bar{\mathbf{x}}^{\mathrm{T}}\hat{\mathbf{M}}\big)\hat{\boldsymbol{p}}_i^{\mathrm{T}} = \bar{\mathbf{x}}\bar{\mathbf{x}}^{\mathrm{T}}\cdot\hat{\mathbf{M}}\hat{\boldsymbol{p}}_i^{\mathrm{T}}. \quad (31)$$

For the first term, note that

$$(\bar{\mathbf{x}}^{\mathrm{T}}\hat{\boldsymbol{p}}_i)\bar{\mathbf{x}}\hat{\mathbf{M}}^{\mathrm{T}} = \bar{\mathbf{x}}\cdot[\bar{\mathbf{x}}^{\mathrm{T}}\hat{\boldsymbol{p}}_i]\cdot\hat{\mathbf{M}}^{\mathrm{T}} = \bar{\mathbf{x}}\bar{\mathbf{x}}^{\mathrm{T}}\cdot\hat{\boldsymbol{p}}_i\hat{\mathbf{M}}^{\mathrm{T}},$$

and then

$$(\bar{\mathbf{x}}^{\mathrm{T}}\hat{\boldsymbol{p}}_i)\bar{\mathbf{x}}\hat{\mathbf{M}}^{\mathrm{T}}\cdot\big(\mathbf{I}-5\hat{\boldsymbol{p}}_i\hat{\boldsymbol{p}}_i^{\mathrm{T}}\big) = \bar{\mathbf{x}}\bar{\mathbf{x}}^{\mathrm{T}}\cdot\hat{\boldsymbol{p}}_i\hat{\mathbf{M}}^{\mathrm{T}}\cdot\big(\mathbf{I}-5\hat{\boldsymbol{p}}_i\hat{\boldsymbol{p}}_i^{\mathrm{T}}\big). \quad (32)$$

Therefore, combing (28), (31) and (32) with $\bar{\mathbf{x}}\bar{\mathbf{x}}^{\mathrm{T}}+\bar{\mathbf{y}}\bar{\mathbf{y}}^{\mathrm{T}}+\bar{\mathbf{z}}\bar{\mathbf{z}}^{\mathrm{T}}=\mathbf{I}$, we get

$$\begin{aligned}&\big(\bar{\mathbf{x}}\hat{\mathbf{M}}^{\mathrm{T}}\big)\mathbb{H}_i^x+\big(\bar{\mathbf{y}}\hat{\mathbf{M}}^{\mathrm{T}}\big)\mathbb{H}_i^y+\big(\bar{\mathbf{z}}\hat{\mathbf{M}}^{\mathrm{T}}\big)\mathbb{H}_i^z\\ &= \left(\hat{\boldsymbol{p}}_i\hat{\mathbf{M}}^{\mathrm{T}}+\hat{\mathbf{M}}\hat{\boldsymbol{p}}_i^{\mathrm{T}}\right)+\big(\hat{\mathbf{M}}^{\mathrm{T}}\hat{\boldsymbol{p}}_i\big)\cdot\left(\mathbf{I}-5\hat{\boldsymbol{p}}_i\hat{\boldsymbol{p}}_i^{\mathrm{T}}\right),\end{aligned} \quad (33)$$

from which it is easy to see that $\mathbb{F}_{\hat{\mathbf{M}}}$ is symmetric.

Appendix B
The Expression of the Matrix $\mathbb{G}^{\mathrm{T}}\mathbb{G}$

Derived from $\mathbf{M}^{\mathrm{T}}\big[\mathbb{G}^{\mathrm{T}}\mathbb{G}\big]\mathbf{M} = \mathrm{tr}\mathbb{F}_{\mathbf{M}}^2$, we can obtain

$$\begin{aligned}\mathbb{G}^{\mathrm{T}}\mathbb{G} = 2\|\boldsymbol{p}\|^2\mathbf{I}-\boldsymbol{p}\boldsymbol{p}^{\mathrm{T}}+\sum_{i=1}^{2}\left(\frac{5}{\|\boldsymbol{p}_i\|^8}-\frac{20(\hat{\boldsymbol{p}}_1\cdot\hat{\boldsymbol{p}}_2)}{\|\boldsymbol{p}_1\|^4\|\boldsymbol{p}_2\|^4}\right)\hat{\boldsymbol{p}}_i\hat{\boldsymbol{p}}_i^{\mathrm{T}}\\ +\frac{25(\hat{\boldsymbol{p}}_1\cdot\hat{\boldsymbol{p}}_2)^2}{\|\boldsymbol{p}_1\|^4\|\boldsymbol{p}_2\|^4}\big[\hat{\boldsymbol{p}}_1\hat{\boldsymbol{p}}_2^{\mathrm{T}}+\hat{\boldsymbol{p}}_2\hat{\boldsymbol{p}}_1^{\mathrm{T}}\big].\end{aligned} \quad (34)$$

APPENDIX C
ERROR ANALYSIS OF GRADIENT FORCE CALCULATION CONSIDERING POSITION DEVIATIONS OF MAGNETIC DIPOLES

To quantify this uncertainty, we consider small deviations in the actuator-magnet positions and examine their influence on the dipole-based force model. Bounds on the perturbed distance and unit direction are first derived and then propagated to the magnetic gradient-force expression.

Let $\boldsymbol{p}_i = \boldsymbol{p} - \boldsymbol{x}_i$ and assume $||\Delta\boldsymbol{p}_i|| << ||\boldsymbol{p}_i||$. Take $r_i = ||\boldsymbol{p}_i|| = ||\boldsymbol{p} - \boldsymbol{x}_i||$ and $\Delta r_i = ||\boldsymbol{p}_i - \Delta\boldsymbol{p}_i|| - ||\boldsymbol{p}_i||$. Applying the Intermediate Value Theorem to the following function (which is differentiable on $(0,1)$ and continuous on $[0,1]$), we have

$$h_i(t) := ||\boldsymbol{p} - (t\Delta\boldsymbol{p}_i + \boldsymbol{x}_i)|| = ||\boldsymbol{p}_i - t\Delta\boldsymbol{p}_i|| \tag{35}$$

we know that there exists some $\theta \in (0,1)$ such that

$$\begin{aligned}\Delta r_i &= h_i(1) - h_i(0)\\ &= \frac{dh_i}{dt}(\theta)(1-0)\\ &= -\frac{(\boldsymbol{p} - \boldsymbol{x}_i - \theta\Delta\boldsymbol{p}_i)\cdot\Delta\boldsymbol{p}_i}{\|\boldsymbol{p} - \boldsymbol{x}_i - \theta\Delta\boldsymbol{p}_i\|}\\ &= -\hat{\boldsymbol{p}}_i^{\,\theta}\cdot\Delta\boldsymbol{p}_i.\end{aligned} \tag{36}$$

Suppose that $\bar{\mathbb{F}}_{\hat{\mathbf{M}}}$ the matrix from measurement, and let $\Delta\mathbb{F}_{\hat{\mathbf{M}}} = \bar{\mathbb{F}}_{\hat{\mathbf{M}}} - \mathbb{F}_{\hat{\mathbf{M}}}$. For convenience, we consider the l^∞-norm of the matrices, that is,

$$\big|\big|[a_{ij}]\big|\big| = \max_{i,j}|a_{ij}|. \tag{37}$$

For estimating the part of the error from $\frac{\left(\hat{\boldsymbol{p}}_i\hat{\mathbf{M}}^{\mathrm{T}} + \hat{\mathbf{M}}\hat{\boldsymbol{p}}_i^{\mathrm{T}}\right)}{\|\boldsymbol{p}_i\|^4} + \frac{\left(\hat{\mathbf{M}}^{\mathrm{T}}\hat{\boldsymbol{p}}_i\right)\cdot\mathbf{I}}{\|\boldsymbol{p}_i\|^4}$, which are the terms of $\mathbb{F}_{\hat{\mathbf{M}}}$ given in equation (6), note that

$$\begin{aligned}&\left\|\frac{\boldsymbol{p}_i - \Delta\boldsymbol{p}_i}{\|\boldsymbol{p}_i - \Delta\boldsymbol{p}_i\|^5} - \frac{\boldsymbol{p}_i}{\|\boldsymbol{p}_i\|^5}\right\|\\ &\le \left\|\boldsymbol{p}_i\left(\frac{1}{\|\boldsymbol{p}_i - \Delta\boldsymbol{p}_i\|^5} - \frac{1}{\|\boldsymbol{p}_i\|^5}\right)\right\| + \frac{\|\Delta\boldsymbol{p}_i\|}{\|\boldsymbol{p}_i - \Delta\boldsymbol{p}_i\|^5}\\ &\le 5\frac{\|\boldsymbol{p}_i\|\left\|\hat{\boldsymbol{p}}_i^{\,\theta}\cdot\Delta\boldsymbol{p}_i\right\|}{\|\boldsymbol{p}_i - \theta\Delta\boldsymbol{p}_i\|^6} + \frac{\|\Delta\boldsymbol{p}_i\|}{\|\boldsymbol{p}_i - \Delta\boldsymbol{p}_i\|^5}\\ &\le 5\frac{\|\boldsymbol{p}_i\|\,\|\Delta\boldsymbol{p}_i\|}{(r_i - \|\Delta\boldsymbol{p}_i\|)^6} + \frac{\|\Delta\boldsymbol{p}_i\|}{(r_i - \|\Delta\boldsymbol{p}_i\|)^5}\\ &= \frac{6r_i - \|\Delta\boldsymbol{p}_i\|}{(r_i - \|\Delta\boldsymbol{p}_i\|)^6}\,\|\Delta\boldsymbol{p}_i\|.\end{aligned} \tag{38}$$

By assuming $\|\Delta\boldsymbol{p}_i\| << r_i$, we may expect

$$6r_i - \|\Delta\boldsymbol{p}_i\| < 7r_i - 7\|\Delta\boldsymbol{p}_i\| \tag{39}$$

and then

$$\left|\left|\frac{\boldsymbol{p}_i - \Delta\boldsymbol{p}_i}{||\boldsymbol{p}_i - \Delta\boldsymbol{p}_i||^5} - \frac{\boldsymbol{p}_i}{||\boldsymbol{p}_i||^5}\right|\right| < \frac{7||\Delta\boldsymbol{p}_i||}{\left(r_i - \|\Delta\boldsymbol{p}_i\|\right)^5}. \tag{40}$$

Therefore, the **Error1** from $\frac{\left(\hat{\boldsymbol{p}}_i\hat{\mathbf{M}}^{\mathrm{T}} + \hat{\mathbf{M}}\hat{\boldsymbol{p}}_i^{\mathrm{T}}\right)}{\|\boldsymbol{p}_i\|^4} + \frac{\left(\hat{\mathbf{M}}^{\mathrm{T}}\hat{\boldsymbol{p}}_i\right)\cdot\mathbf{I}}{\|\boldsymbol{p}_i\|^4}$ is bounded by

$$\textbf{Error1} \le 3\sum_{i=\pm}\frac{7||\Delta\boldsymbol{p}_i||}{\left(r_i - \|\Delta\boldsymbol{p}_i\|\right)^5} = \sum_{i=\pm}\frac{21\cdot||\Delta\boldsymbol{p}_i||}{\left(r_i - \|\Delta\boldsymbol{p}_i\|\right)^5} \tag{41}$$

For the error from $(\hat{\mathbf{M}}\cdot\hat{\boldsymbol{p}}_i)\frac{\hat{\boldsymbol{p}}_i\hat{\boldsymbol{p}}_i^{\mathsf{T}}}{||\boldsymbol{p}_i||^4}$, define $\Delta\hat{\boldsymbol{p}}_i = \frac{\boldsymbol{p}_i - \Delta\boldsymbol{p}_i}{||\boldsymbol{p}_i - \Delta\boldsymbol{p}_i||} - \frac{\boldsymbol{p}_i}{||\boldsymbol{p}_i||}$. Then

$$\begin{aligned}&\left\|\frac{\boldsymbol{p}_i - \Delta\boldsymbol{p}_i}{\|\boldsymbol{p}_i - \Delta\boldsymbol{p}_i\|} - \frac{\boldsymbol{p}_i}{\|\boldsymbol{p}_i\|}\right\|\\ &\le \|\boldsymbol{p}_i\|\left|\frac{1}{\|\boldsymbol{p}_i - \Delta\boldsymbol{p}_i\|} - \frac{1}{\|\boldsymbol{p}_i\|}\right| + \frac{\|\Delta\boldsymbol{p}_i\|}{\|\boldsymbol{p}_i - \Delta\boldsymbol{p}_i\|}\\ &= \|\boldsymbol{p}_i\|\frac{\left|\hat{\boldsymbol{p}}_i^{\,\theta}\cdot\Delta\boldsymbol{p}_i\right|}{\|\boldsymbol{p}_i - \theta\Delta\boldsymbol{p}_i\|^2} + \frac{\|\Delta\boldsymbol{p}_i\|}{\|\boldsymbol{p}_i - \Delta\boldsymbol{p}_i\|}\\ &\le \frac{2r_i - \|\Delta\boldsymbol{p}_i\|}{(r_i - \|\Delta\boldsymbol{p}_i\|)^2}\,\|\Delta\boldsymbol{p}_i\|.\end{aligned} \tag{42}$$

From $\|\Delta\boldsymbol{p}_i\| << r_i$ we expect

$$2r_i - \|\Delta\boldsymbol{p}_i\| \le 3r_i - 3\|\Delta\boldsymbol{p}_i\|, \tag{43}$$

and then

$$||\Delta\hat{\boldsymbol{p}}_i|| = \left|\left|\frac{\boldsymbol{p}_i - \Delta\boldsymbol{p}_i}{||\boldsymbol{p}_i - \Delta\boldsymbol{p}_i||} - \frac{\boldsymbol{p}_i}{||\boldsymbol{p}_i||}\right|\right| \le \frac{3||\Delta\boldsymbol{p}_i||}{r_i - \|\Delta\boldsymbol{p}_i\|}. \tag{44}$$

As a result,

$$\begin{aligned}&\hat{\mathbf{M}}^{\mathsf{T}}(\hat{\boldsymbol{p}}_i + \Delta\hat{\boldsymbol{p}}_i)\frac{(\hat{\boldsymbol{p}}_i + \Delta\hat{\boldsymbol{p}}_i)(\hat{\boldsymbol{p}}_i + \Delta\hat{\boldsymbol{p}}_i)^{\mathsf{T}}}{\|\boldsymbol{p}_i - \Delta\boldsymbol{p}_i\|^4}\\ &= (\hat{\mathbf{M}}\cdot\hat{\boldsymbol{p}}_i)\frac{\hat{\boldsymbol{p}}_i\hat{\boldsymbol{p}}_i^{\mathsf{T}}}{\|\boldsymbol{p}_i - \Delta\boldsymbol{p}_i\|^4} + \underbrace{(\hat{\mathbf{M}}\cdot\Delta\hat{\boldsymbol{p}}_i)\frac{\hat{\boldsymbol{p}}_i\hat{\boldsymbol{p}}_i^{\mathsf{T}}}{\|\boldsymbol{p}_i - \Delta\boldsymbol{p}_i\|^4} + \cdots}_{\text{3 terms containing one }\Delta\hat{\boldsymbol{p}}_i}\\ &+ \underbrace{(\hat{\mathbf{M}}\cdot\hat{\boldsymbol{p}}_i)\frac{\Delta\hat{\boldsymbol{p}}_i\Delta\hat{\boldsymbol{p}}_i^{\mathsf{T}}}{\|\boldsymbol{p}_i - \Delta\boldsymbol{p}_i\|^4} + \cdots}_{\text{3 terms containing two }\Delta\hat{\boldsymbol{p}}_i} + (\hat{\mathbf{M}}\cdot\Delta\hat{\boldsymbol{p}}_i)\frac{\Delta\hat{\boldsymbol{p}}_i\Delta\hat{\boldsymbol{p}}_i^{\mathsf{T}}}{\|\boldsymbol{p}_i - \Delta\boldsymbol{p}_i\|^4}.\end{aligned} \tag{45}$$

and then

$$\begin{aligned}&\hat{\mathbf{M}}^{\mathsf{T}}(\hat{\boldsymbol{p}}_i + \Delta\hat{\boldsymbol{p}}_i)\frac{(\hat{\boldsymbol{p}}_i + \Delta\hat{\boldsymbol{p}}_i)(\hat{\boldsymbol{p}}_i + \Delta\hat{\boldsymbol{p}}_i)^{\mathsf{T}}}{\|\boldsymbol{p}_i - \Delta\boldsymbol{p}_i\|^4} - (\hat{\mathbf{M}}\cdot\hat{\boldsymbol{p}}_i)\frac{\hat{\boldsymbol{p}}_i\hat{\boldsymbol{p}}_i^{\mathsf{T}}}{\|\boldsymbol{p}_i\|^4}\\ &= (\hat{\mathbf{M}}\cdot\hat{\boldsymbol{p}}_i)\left(\frac{\hat{\boldsymbol{p}}_i\hat{\boldsymbol{p}}_i^{\mathsf{T}}}{\|\boldsymbol{p}_i - \Delta\boldsymbol{p}_i\|^4} - \frac{\hat{\boldsymbol{p}}_i\hat{\boldsymbol{p}}_i^{\mathsf{T}}}{\|\boldsymbol{p}_i\|^4}\right)\\ &+ \underbrace{\frac{(\hat{\mathbf{M}}\cdot\Delta\hat{\boldsymbol{p}}_i)\hat{\boldsymbol{p}}_i\hat{\boldsymbol{p}}_i^{\mathsf{T}}}{\|\boldsymbol{p}_i - \Delta\boldsymbol{p}_i\|^4} + \cdots}_{\text{3 terms containing one }\Delta\hat{\boldsymbol{p}}_i} + \underbrace{\frac{(\hat{\mathbf{M}}\cdot\hat{\boldsymbol{p}}_i)\Delta\hat{\boldsymbol{p}}_i\Delta\hat{\boldsymbol{p}}_i^{\mathsf{T}}}{\|\boldsymbol{p}_i - \Delta\boldsymbol{p}_i\|^4} + \cdots}_{\text{3 terms containing two }\Delta\hat{\boldsymbol{p}}_i}\\ &+ \frac{(\hat{\mathbf{M}}\cdot\Delta\hat{\boldsymbol{p}}_i)\Delta\hat{\boldsymbol{p}}_i\Delta\hat{\boldsymbol{p}}_i^{\mathsf{T}}}{\|\boldsymbol{p}_i - \Delta\boldsymbol{p}_i\|^4}.\end{aligned} \tag{46}$$

For the term $\frac{(\hat{\mathbf{M}}\cdot\hat{\boldsymbol{p}}_i)\hat{\boldsymbol{p}}_i\hat{\boldsymbol{p}}_i^{\mathsf{T}}}{||\boldsymbol{p}_i - \Delta\boldsymbol{p}_i||^4} - \frac{(\hat{\mathbf{M}}\cdot\hat{\boldsymbol{p}}_i)\hat{\boldsymbol{p}}_i\hat{\boldsymbol{p}}_i^{\mathsf{T}}}{||\boldsymbol{p}_i||^4}$

$$\begin{aligned}&\left\|\frac{(\hat{\mathbf{M}}\cdot\hat{\boldsymbol{p}}_i)\,\hat{\boldsymbol{p}}_i\hat{\boldsymbol{p}}_i^{\mathsf{T}}}{\|\boldsymbol{p}_i - \Delta\boldsymbol{p}_i\|^4} - \frac{(\hat{\mathbf{M}}\cdot\hat{\boldsymbol{p}}_i)\,\hat{\boldsymbol{p}}_i\hat{\boldsymbol{p}}_i^{\mathsf{T}}}{\|\boldsymbol{p}_i\|^4}\right\|\\ &\le \left\|\frac{1}{\|\boldsymbol{p}_i - \Delta\boldsymbol{p}_i\|^4} - \frac{1}{\|\boldsymbol{p}_i\|^4}\right\|\cdot\|(\hat{\mathbf{M}}\cdot\hat{\boldsymbol{p}}_i)\hat{\boldsymbol{p}}_i\hat{\boldsymbol{p}}_i^{\mathsf{T}}\|\\ &= \frac{5\left\|\hat{\boldsymbol{p}}_i^{\,\theta}\cdot\Delta\boldsymbol{p}_i\right\|}{\|\boldsymbol{p}_i - \theta\Delta\boldsymbol{p}_i\|^5}\\ &\le \frac{5\|\Delta\boldsymbol{p}_i\|}{(r_i - \|\Delta\boldsymbol{p}_i\|)^5}.\end{aligned} \tag{47}$$

For the other terms, use the estimation $||\Delta\hat{\boldsymbol{p}}_i|| \leq \frac{3||\Delta\boldsymbol{p}_i||}{r_i-\|\Delta\boldsymbol{p}_i\|}$ obtained above and get

$$\begin{aligned}
&\Bigg\| \underbrace{(\hat{\mathbf{M}}\cdot\Delta\hat{\boldsymbol{p}}_i)\frac{\hat{\boldsymbol{p}}_i\hat{\boldsymbol{p}}_i^{\mathsf{T}}}{\|\boldsymbol{p}_i-\Delta\boldsymbol{p}_i\|^4}+\cdots}_{3 \text{ terms with one } \Delta\hat{\boldsymbol{p}}_i} \Bigg\| \\
&+ \Bigg\| \underbrace{(\hat{\mathbf{M}}\cdot\hat{\boldsymbol{p}}_i)\frac{\Delta\hat{\boldsymbol{p}}_i\Delta\hat{\boldsymbol{p}}_i^{\mathsf{T}}}{\|\boldsymbol{p}_i-\Delta\boldsymbol{p}_i\|^4}\Bigg\|+\cdots}_{3 \text{ terms with two } \Delta\hat{\boldsymbol{p}}_i} \\
&+ \left\|(\hat{\mathbf{M}}\cdot\Delta\hat{\boldsymbol{p}}_i)\frac{\Delta\hat{\boldsymbol{p}}_i\Delta\hat{\boldsymbol{p}}_i^{\mathsf{T}}}{\|\boldsymbol{p}_i-\Delta\boldsymbol{p}_i\|^4}\right\| \\
&\leq \frac{3\|\Delta\hat{\boldsymbol{p}}_i\|}{\|\boldsymbol{p}_i-\Delta\boldsymbol{p}_i\|^4}+\frac{3\|\Delta\hat{\boldsymbol{p}}_i\|^2}{\|\boldsymbol{p}_i-\Delta\boldsymbol{p}_i\|^4}+\frac{\|\Delta\hat{\boldsymbol{p}}_i\|^3}{\|\boldsymbol{p}_i-\Delta\boldsymbol{p}_i\|^4} \\
&\leq \frac{9\|\Delta\boldsymbol{p}_i\|}{(r_i-\|\Delta\boldsymbol{p}_i\|)^5}+\frac{27\|\Delta\boldsymbol{p}_i\|^2}{(r_i-\|\Delta\boldsymbol{p}_i\|)^6}+\frac{27\|\Delta\boldsymbol{p}_i\|^3}{(r_i-\|\Delta\boldsymbol{p}_i\|)^7}
\end{aligned} \tag{48}$$

If we expect from $\|\Delta\boldsymbol{p}_i\| << r_i$

$$\frac{||\Delta\boldsymbol{p}_i||}{r_i-\|\Delta\boldsymbol{p}_i\|}<\frac{1}{N}, \tag{49}$$

then

$$\begin{aligned}
&\frac{9\|\Delta\boldsymbol{p}_i\|}{(r_i-\|\Delta\boldsymbol{p}_i\|)^5}+\frac{27\|\Delta\boldsymbol{p}_i\|^2}{(r_i-\|\Delta\boldsymbol{p}_i\|)^6}+\frac{27\|\Delta\boldsymbol{p}_i\|^3}{(r_i-\|\Delta\boldsymbol{p}_i\|)^7} \\
&\leq \frac{\left(9+\frac{27}{N}+\frac{27}{N^2}\right)\|\Delta\boldsymbol{p}_i\|}{(r_i-\|\Delta\boldsymbol{p}_i\|)^5}
\end{aligned} \tag{50}$$

Combining (47) and (50) yields an estimation for the **Error2** from $\sum_{i=\pm}(\hat{\mathbf{M}}\cdot\hat{\boldsymbol{p}}_i)\frac{\hat{\boldsymbol{p}}_i\hat{\boldsymbol{p}}_i^{\mathsf{T}}}{||\boldsymbol{p}_i||^4}$:

$$\textbf{Error2} \leq \sum_{i=\pm}\frac{(14+\frac{27}{N}+\frac{27}{N^2})\cdot||\Delta\boldsymbol{p}_i||}{\left(r_i-\|\Delta\boldsymbol{p}_i\|\right)^5}. \tag{51}$$

The upper limit of the total error of gradient force applied on the UMD is given as

$$\begin{aligned}
\|\Delta\mathbf{F}\| &= \mathcal{K}\|\Delta\mathbb{F}_{\hat{\mathbf{M}}}\| \\
&\leq \mathcal{K}\big(\textbf{Error1}+5*\textbf{Error2}\big) \\
&\leq \frac{3\mu_0\|\mathbf{M}\|\|\mathbf{m}\|}{4\pi}\sum_{i=1}^{2}\frac{\left(91+\frac{135}{N}+\frac{135}{N^2}\right)\|\Delta\boldsymbol{p}_i\|}{\left(r_i-\|\Delta\boldsymbol{p}_i\|\right)^5}
\end{aligned} \tag{52}$$

ACKNOWLEDGMENT

The research is supported by China Scholarship Council, Europe Research Council (ERC) European Union's Horizon2020 Research and innovation program (no.866494-project MAESTRO), Research development Fund of Xi'an Jiaotong Liverpool University (RDF-24-01-086), Wenzhou Science and Technology Major Project (ZG2024005), Research Start-up Fund of Wenzhou University of Technology (10007000080175), Wenzhou Municipal Key Science and Research Program (ZG2023023), Wenling Municipal Key Science and Research Program (2023G00009), General project of Zhejiang Health and Pharmaceutical Science and Technology Plan (2025KY466), and Natural Science Foundation of Zhejiang province (LQN25E050031).

REFERENCES

[1] A. Menciassi, E. Sinibaldi, V. Pensabene, and P. Dario, "From miniature to nano robots for diagnostic and therapeutic applications," in *2010 Annual International Conference of the IEEE Engineering in Medicine and Biology*. IEEE, 2010, pp. 1954–1957.

[2] S. Ornes, "Inner workings: Medical microrobots have potential in surgery, therapy, imaging, and diagnostics," *Proceedings of the National Academy of Sciences*, vol. 114, no. 47, pp. 12 356–12 358, 2017.

[3] J. Leclerc, H. Zhao, D. Bao, and A. T. Becker, "In vitro design investigation of a rotating helical magnetic swimmer for combined 3-d navigation and blood clot removal," *IEEE Transactions on Robotics*, vol. 36, no. 3, pp. 975–982, 2020.

[4] I. S. Khalil, A. Adel, D. Mahdy, M. M. Micheal, M. Mansour, N. Hamdi, and S. Misra, "Magnetic localization and control of helical robots for clearing superficial blood clots," *APL bioengineering*, vol. 3, no. 2, p. 026104, 2019.

[5] W. Chen, Y. Wen, X. Fan, M. Sun, C. Tian, M. Yang, and H. Xie, "Magnetically actuated intelligent hydrogel-based child-parent microrobots for targeted drug delivery," *Journal of Materials Chemistry B*, vol. 9, no. 4, pp. 1030–1039, 2021.

[6] G. Dogangil, O. Ergeneman, J. J. Abbott, S. Pané, H. Hall, S. Muntwyler, and B. J. Nelson, "Toward targeted retinal drug delivery with wireless magnetic microrobots," in *2008 IEEE/RSJ International Conference on Intelligent Robots and Systems*. IEEE, 2008, pp. 1921–1926.

[7] J. J. Abbott, K. E. Peyer, M. C. Lagomarsino, L. Zhang, L. Dong, I. K. Kaliakatsos, and B. J. Nelson, "How should microrobots swim?" *The international journal of Robotics Research*, vol. 28, no. 11-12, pp. 1434–1447, 2009.

[8] C. J. Zimmermann, A. J. Petruska, K. B. Neeves, and D. W. Marr, "Coupling magnetic torque and force for colloidal microbot assembly and manipulation," *Advanced Intelligent Systems*, vol. 5, no. 12, p. 2300332, 2023.

[9] D. Son, M. C. Ugurlu, and M. Sitti, "Permanent magnet array–driven navigation of wireless millirobots inside soft tissues," *Science Advances*, vol. 7, no. 43, p. eabi8932, 2021.

[10] A. W. Mahoney and J. J. Abbott, "Managing magnetic force applied to a magnetic device by a rotating dipole field," *Applied Physics Letters*, vol. 99, no. 13, 2011.

[11] ——, "Generating rotating magnetic fields with a single permanent magnet for propulsion of untethered magnetic devices in a lumen," *IEEE Transactions on Robotics*, vol. 30, no. 2, pp. 411–420, 2013.

[12] A. W. Mahoney, S. E. Wright, and J. J. Abbott, "Managing the attractive magnetic force between an untethered magnetically actuated tool and a rotating permanent magnet," in *2013 IEEE International Conference on Robotics and Automation*. IEEE, 2013, pp. 5366–5371.

[13] A. Hosney, A. Klingner, S. Misra, and I. S. Khalil, "Propulsion and steering of helical magnetic microrobots using two synchronized rotating dipole fields in three-dimensional space," in *2015 IEEE/RSJ International Conference on Intelligent Robots and Systems (IROS)*. IEEE, 2015, pp. 1988–1993.